JLR RESEARCH ARTICLE

# Diet-induced obesity dampens the temporal oscillation of hepatic mitochondrial lipids

**Rashi Jain, Rajprabu Rajendran, and Sona Rajakumari***

Department of Developmental Biology and Genetics, Indian Institute of Science, Bengaluru, Karnataka, India

**Abstract** **Mitochondria play a pivotal role in energy homeostasis and regulate several metabolic pathways. The inner and outer membrane of mitochondria comprises unique lipid composition and proteins that are essential to form electron transport chain complexes, orchestrate oxidative phosphorylation, β-oxidation, ATP synthesis, etc. As known, diet-induced obesity affects mitochondrial function, dynamics, and mitophagy, which are governed by circadian clock machinery. Though DIO impairs the interplay between circadian oscillation and lipid metabolism, the impact of DIO on mitochondrial membrane lipid composition and their temporal oscillation is unknown. Thus, we investigated the diurnal oscillation of liver mitochondrial lipidome at various Zeitgeber times using quantitative lipidomics. Our data suggested that obesity disrupted lipid accumulation profiles and diminished the oscillating lipid species in the hepatic mitochondria. Strikingly, HFD manifested a more homogenous temporal oscillation pattern in phospholipids regardless of possessing different fatty acyl-chain lengths and degrees of unsaturation. In particular, DIO impaired the circadian rhythmicity of phosphatidyl ethanolamine, phosphatidyl choline, phosphatidyl serine, and ether-linked phosphatidyl ethanolamine. Also, DIO altered the rhythmic profile of PE/PC, ePE/PC, PS/PC ratio, and key proteins related to mitochondrial function, dynamics, and quality control. Since HFD dampened lipid oscillation, we examined whether the diurnal oscillation of mitochondrial lipids synchronized with mitochondrial function. Also, our data emphasized that acrophase of mitochondrial lipids synchronized with increased oxygen consumption rate and Parkin levels at ZT16 in chow-fed mice. Our study revealed that obesity altered the mitochondrial lipid composition and hampered the rhythmicity of mitochondrial lipids, oxygen consumption rate, and Parkin levels in the liver.**

**Supplementary key words** Circadian rhythm • Temporal oscillation • High-fat diet • Membrane lipids • Diet-induced obesity • MASLD • OXPHOS • Mitochondrial lipidome

The daily 24-h light-dark (LD) cycle is the most important reliable cue to entrain the circadian oscillation system, and it synchronizes several physiological processes, such as feeding behavior, rest and activity, energy storage and energy utilization, etc. of various tissues and organs with each other and with the LD cycles. In mammals, the molecular machinery of circadian rhythm comprises a transcriptional-translational feedback loop that is hierarchically orchestrated by the suprachiasmatic nucleus (SCN) of the hypothalamus, the master pacemaker (1, 2). The SCN receives the photic cues detected by the retina through the retinohypothalamic tract and transmits the signal via its neurons to all peripheral organs and cells of the body to alter the expression of clock genes (3, 4). This hierarchical network ensures that all our bodily activities, including sleep and wake cycles, body temperature, blood pressure, circulating hormones, and metabolism, are entrained with circadian rhythm (5). While SCN controls the temporal oscillation of behavioral processes, several research studies reported that perturbing the function of clock machinery and/or interrupting circadian rhythm severely affects systemic energy homeostasis in mammals (6–8).

The transcriptional feedback circuit governs the molecular clock machinery in mammals, comprising several genes. Among them, the CLOCK: BMAL1 forms a heterodimer complex and binds to specific DNA elements referred to as E-boxes (5′-CACGTG-3′) and E′-boxes (5′-CACGTT-3′) in the promoters and activate transcription of its target genes, *Per* (*Per1* and *Per2*) and *Cry* (*Cry1* and *Cry2*) (9–14). These genes establish the negative limb of the transcriptional feedback loop by forming a PER: CRY dimer complex and inhibit the transcriptional activity of the CLOCK: BMAL complex (15, 16). Besides, the turnover rate of PER and CRY proteins adds another layer of complexity to maintain the repression phase and replenish a new transcription cycle. While CLOCK: BMAL1 forms a negative feedback loop, the REV-ERB and ROR proteins also establish yet another negative regulation by competing for retinoic acid-related orphan receptor response element–binding sites within the *Bmal1* promoter. Although REV-ERBα

*For correspondence: Sona Rajakumari, sona@iisc.ac.in.



 https://doi.org/10.1016/j.jlr.2025.100790

binding onto the retinoic acid-related orphan receptor response element site diminishes the *Bmal1* expression, binding of RORα onto the same site promotes *Bmal1* expression levels, suggesting that both proteins compete with each other for the same site (17–20). As well known, both proteins play a critical role in lipid metabolism and, in particular, render their function in regulating circadian rhythmicity lipid metabolism by governing *Bmal1* expression (21, 22).

Numerous findings suggest that systemic lipid homeostasis is governed by the master clock and through overlapping transcription networks tethered to the internal circadian clock machinery (23–27). However, diet-induced obesity (DIO) or metabolic dysfunction-associated steatotic liver disease drastically alters the circadian rhythmicity of key nuclear receptors, clock transcription factors, and clock-controlled lipid metabolism genes in the liver (28, 29). Recent studies revealed that DIO altered lipid profiles in the liver using lipid mass spectrometry analyses (30, 31). As lipids decorate the membranes of all organelles, even salient variations in the membrane lipid composition affect the functional capacity of organelles. In particular, mitochondrial lipid composition is crucial for many processes, such as mitochondrial oxidative phosphorylation, β-oxidation, fission-fusion dynamics, mitophagy, etc (32–35). Thus, altering mitochondrial phospholipid composition leads to deleterious effects on oxidative phosphorylation (OXPHOS) complex protein organization, abnormal mitochondrial cristae, and bioenergetic properties of mitochondria and causes metabolic diseases (33, 36, 37). Though elegant lipidomic studies reported the changes in the circadian rhythmicity of lipids and their spatial organization at the organelle level (23), how DIO affects the temporal organization of mitochondrial lipids oscillation and mitochondrial dynamics is unknown. Also, whether the oscillating lipids are associated with temporal rhythmicity of mitochondrial homeostasis in the liver is unclear.

Therefore, we profiled the liver mitochondrial lipidome of chow- and high fat diet (HFD)-fed mice using quantitative lipidomics. Our study demonstrates that DIO severely perturbed the lipid composition and circadian oscillation of mitochondrial lipid species. The DIO mice displayed an altered rhythmicity of lipid biosynthetic genes, mitochondrial function, and mitophagy markers. Hence, studying the lipid profile of mitochondrial membranes during DIO-induced liver disease progression that complies with the circadian oscillation in the liver could pave the way for understanding obesity-induced mitochondrial dysfunction.

## MATERIALS AND METHODS

### Animal studies

All animal handling procedures and experiments were reviewed and approved by the Institutional Animal Ethics Committee governed by the Central Animal Facility, Indian Institute of Science (CAF, IISc). The approval committee was constituted as per article number 13 of the Committee for Control and Supervision of Experiments on Animals (CPCSEA), Government of India. Male C57BL/6 mice were maintained at a controlled temperature of 22°C ± 2 under a standard 12-h LD cycle and fed ad libitum with standard rodent chow containing 10 kcal% or 60 kcal% in case of a high-fat diet. For the DIO study, C57BL/6 male mice (5–6 weeks) were challenged for 10- to 12-weeks of HFD. At the terminal stage of the experiment, mice were euthanized using carbon dioxide inhalation, and tissues were collected at 4-h intervals (ZT0, 4, 8, 12, 16, and 20), with six mice per time point. To reduce the impact of light cues on circadian rhythms, animals were sacrificed within 10 minutes of their scheduled tissue collection time. Zeitgeber time (ZT) 0 corresponded to lights-on and ZT12 to lights-off in the animal facility.

### Mitochondria isolation from the liver

Mitochondria were isolated from liver tissues using the method described previously (38). Liver tissues were harvested from mice (n = 6 mice/ZT point) and rinsed thoroughly in ice-cold PBS 3 to 4 times. To generate each biological replicate, tissues from two mice were pooled, and thus, each ZT point consisted of three independent biological replicates per group. The tissue was minced finely in mitochondrial isolation buffer I (6.7 ml of 1 M sucrose/100 ml, 50 mM Tris/HCl, 50 mM KCl, 10 mM EDTA; pH 7.4) supplemented with 0.4% BSA and then homogenized using a glass homogenizer with 80–90 strokes with all steps carried out on ice. Both groups were processed identically to minimize any discrepancies in the data. The homogenate was centrifuged at 600 *g* for 10 mign at 4°C. The supernatant was carefully aspirated without disturbing the lipid layer and centrifuged at 7000 *g* for 10 min at 4°C. After discarding the supernatant, the resulting pellet was washed with ice-cold mitochondrial isolation buffer II (0.25 M sucrose, 3 mM EGTA/Tris, and 10 mM Tris/HCl; pH 7.4). The washed mitochondrial pellet was finally resuspended to the desired volume in mitochondrial isolation buffer II, and protein concentration was measured using Pierce™ BCA Protein Assay Kit to prepare for lipid extraction.

### Lipid extraction

Lipids were extracted from isolated liver mitochondria (n = 3 biological replicates per ZT point, where each biological replicate was generated by pooling liver tissue from two mice) using the modified Bligh and Dyer method (39). Briefly, isolated mitochondria (200 μg of protein/sample) were subjected to a mixture of chloroform containing 0.01% butylated hydroxytoluene and methanol (1:2, v/v). Phase separation was induced by adding acidified water and chloroform (1:1, v/v), followed by mixing and centrifugation at 5,000 rpm for 10 min. The lower chloroform layer was collected, and lipids were re-extracted by adding 1 ml of chloroform, followed by another round of centrifugation and collection of the chloroform phase. The pooled chloroform extracts were subsequently washed with 1 M KCl and then with acidified water. Finally, the washed chloroform layer was dried under a vacuum for further lipidomic analysis.

### Quantitative lipidomics study

The quantitative lipidome analyses were performed at the Kansas Lipidomics Research Center Analytical Laboratory.

Lipid molecular species were detected using electrospray ionization. Mass spectrometry was performed on a Xevo TQ-S micro–Tandem Quadrupole Mass Spectrometer (Waters corporation) via direct infusion, with a sample infusion rate of 30 µl per minute from a sample loop. As ions transitioned into the gaseous phase and traversed the tandem mass spectrometer's ion path, an applied electric field directed ions with specific mass/charge (m/z) ratios to the detector. Phosphatidylcholine (PC), sphingomyelin (SM), phosphatidylserine (PS), phosphatidylethanolamine (PE), and lysophosphatidylethanolamine (LPE) species were analyzed as singly-charged positive [M + H]+ ions, while phosphatidylinositol (PI), phosphatidic acid (PA), and PS were detected as singly-charged [M + NH4]+ ions. Precursor ion scans or neutral loss scans were used to identify and quantify lipid species within specific head group classes. Corrections for isotopic overlap were applied before quantifying the spectral peaks in relation to a set of internal standards. These standards included 0.60 nmol PC (12:0/12:0), 0.60 nmol PC (24:1/24:1), 0.30 nmol PE (12:0/12:0), 0.30 nmol PE (phytanoyl/phytanoyl), that is, PE (20:0/20:0), 0.30 nmol LPE (14:0), 0.30 nmol LPE (18:0), 0.30 nmol LPG (14:0), 0.30 nmol PA (14:0/14:0), 0.30 nmol PA (phytanoyl/phytanoyl), that is, PA (20:0/20:0), 0.20 nmol PS (14:0/14:0), 0.20 nmol PS (phytanoyl/phytanoyl), that is, PS (20:0/20:0), 0.23 nmol PI (16:0/18:0), and 0.015 nmol cardiolipin (CL, 14:0/14:0/14:0/14:0). As described by Zhou *et al.*, lipidomic data were processed utilizing the LipidomeDB Data Calculation Environment (40). The data for each lipid molecular species is presented as nmol/mg protein for polar lipids. To ensure data quality and reproducibility and to avoid any artifacts, the coefficient of variation, defined as the ratio of the standard deviation to the mean (SD/Mean), was calculated for each lipid species across all diets and ZT points. A threshold of 0.3 was used as the cutoff for use in further statistical analyses. Also, lipids with an average value < 0.0005 nmol were below the detection limit and were not analyzed further (41–46). The list of lipid species that failed to meet this requirement is provided in the supplemental data (Excel sheet 1).

## Lipidomics data analyses

Normalized lipid values were calculated by dividing the raw lipid measurements at each specific ZT by the average lipid value across all ZT points for that day. Principal component analysis (PCA) was performed on scaled lipidome data for all six-time points using the ggplot2, stats, and dplyr packages in R. For bar graphs illustrating lipid concentrations in chow-fed and HFD-fed groups; the daily average was calculated using measurements from six ZT points. Heatmaps were generated using the Pheatmap package, while the correlation matrices were computed with the cor function from base R and visualized using the corrplot function. Hierarchical clustering for daily lipid oscillation profile of the normalized lipidomics data was conducted based on Euclidean distance using the "ward. D2" method, implemented via the hclust from the stats package. The number of clusters was decided by manually inspecting the distance matrix, excluding those with fewer than five lipid species. Lipid pairs were grouped based on correlation strength, measured using Pearson correlation coefficients, for chow- and HFD-fed mice. These pairs were further categorized by lipid class, acyl chain length similarity, and degree of unsaturation. To ensure statistical robustness, categories containing fewer than two lipid pairs were excluded from the analysis. For fatty acid chain length analysis, lipid pairs within the same class were classified as within-group if their chain length differed by no more than two carbons. Similarly, for the degree of unsaturation, lipid pairs were considered within the group if they differed by no more than one double bond. Network plots were constructed using the igraph and circlize packages in R, with lipid pairs filtered based on a correlation threshold of >0.8 and a false discovery rate < 0.01.

## Circadian lipidomics analysis

The rhythmicity of lipid levels and mRNA expression was analyzed using the nonparametric test JTK_CYCLE, with a 20–24 h period across six ZT points (47). Lipids were considered rhythmic if the Bonferroni-corrected *P*-value was less than 0.05.

## Western blot analysis

Whole liver and mitochondrial proteins were extracted in RIPA buffer (1% NP-40, 0.5% sodium deoxycholate, 150 mM NaCl, 50 mM Tris-Cl (pH 7.5), and 0.1% SDS) supplemented with protease inhibitor cocktail (cOmplete; Roche) and 1 mM phenylmethyl sulfonyl fluoride. The protein estimation was done using Pierce™ BCA Protein Assay Kit with BSA as standard. Samples were heated at 95°C for 5 min in Laemmli sample buffer. An equal amount of lysate or mitochondrial fraction was separated onto a 10% SDS-PAGE and transferred to PVDF membranes. After blocking with 5% skim milk, the membranes were incubated with primary antibodies overnight at 4°C, followed by incubation with horseradish peroxidase-conjugated secondary antibodies. The immunoblots were then developed using Clarity western blotting ECL substrate (Bio-Rad). The sources of primary antibodies are listed in supplemental Table S1.

## Real-time qPCR

Total RNA was isolated from liver samples using RNAiso plus reagent (Takara). The aqueous layer containing RNA was collected and RNA was precipitated using isopropanol. The resulting RNA pellet was washed with ethanol and resuspended in RNase-free water. One microgram of RNA from each sample was reverse transcribed to complementary DNA using a high-capacity cDNA synthesis kit (Applied Biosystems). Quantitative real-time PCR was performed with the iTaq universal SYBR green mix (Bio-Rad) on the CFX384 Real-Time system (Bio-Rad). For each sample, duplicate test reactions were analyzed to assess the expression of genes of interest, and results were normalized to TATA-binding protein (*Tbp*) mRNA. The sequences of the indicated primers are presented in supplemental Table S2.

## Oxygen consumption assay

As described earlier, mitochondria isolated from liver tissue at ZT4 and ZT16 from chow-fed and HFD-fed mice, respectively. Mitochondria were resuspended in respiratory buffer containing 225 mM sucrose, 75 mM mannitol, 10 mM Tris-HCl (pH 7.4), 10 mM KCl, 10 mM $KH_2PO_4$, 5 mM $MgCl_2$, and 1 mg/ml fatty acids-free BSA (pH 7.4). Oxygen consumption rate (OCR) was measured using the Strathkelvin Oxygen electrode (MT200A) in the presence of 2 mM pyruvate for 2–3 min. The protein concentration of samples was measured using a Pierce BCA protein assay kit, which was utilized for OCR data normalization.

### Statistical analysis

All experiments were conducted for a minimum of three times unless mentioned otherwise. Differences between groups were analyzed using either an unpaired two-tailed Student's *t* test or a two-way ANOVA. Data are presented as mean ± SEM. Statistical significance was set at $*P \leq 0.05$, $**P < 0.01$, $***P < 0.001$. Graphs and statistical analyses were performed using GraphPad Prism software version 5.0.

## RESULTS

### DIO altered the mitochondrial lipid composition of the liver

As reported, DIO leads to mitochondrial dysfunction by altering mitochondrial membrane composition and promotes metabolic diseases, including obesity, metabolic dysfunction-associated steatotic liver disease, type 2 diabetes, etc (48–51). Though multiple lipidomics studies (30, 31) revealed the lipid profile of liver lysate, the comparative analyses of mitochondrial-specific lipids and their circadian oscillation pattern of chow and HFD mice are unknown. Thus, we first set out to analyze the lipid composition of liver mitochondria from chow- and HFD-challenged mice (**Fig. 1**A). As anticipated, the fractionated mitochondria from the liver showed an enrichment for voltage-dependent anion-selective channel (VDAC), mitochondrial-specific protein. Further, we examined the presence of other organelle marker proteins such as ERP72 (endoplasmic reticulum), GAPDH (cytosol), and MATR3 (nucleus), respectively. Although we detected other organelle markers in our mitochondrial fractionation, their presence is significantly low and constant throughout the LD cycle. On the contrary,

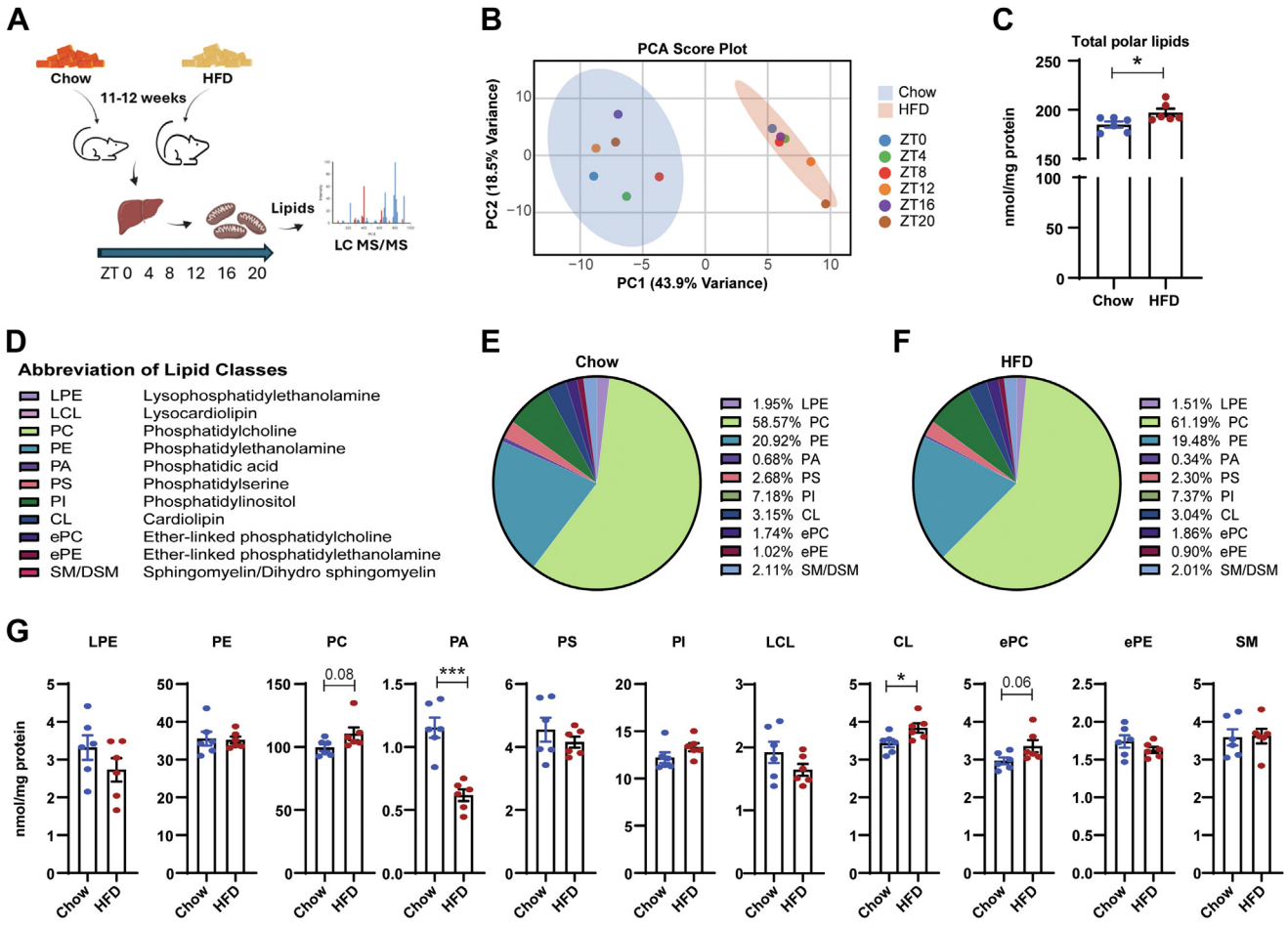


**Fig. 1.** High-fat diet-induced mitochondrial lipid remodeling in the liver. A: Experimental schematic: C57BL/6 mice (5–6 weeks old) were fed either a chow or a high-fat diet (HFD) for 11–12 weeks. Liver tissues were collected every 4 h over a 24-h period within 10 min at each ZT point (six-time points, n = 6 mice/ZT point). Livers from two mice were pooled to isolate mitochondria using differential centrifugation, resulting in three biological replicates per ZT point. Lipids were extracted from these mitochondrial samples and analyzed via shotgun lipidomics. B: Principal component analysis (PCA) of lipidomic profiles distinguishing the two diet groups. Each data point represents ZT0, 4, 8, 12, 16, and 20. C: Total polar lipid concentration in the liver mitochondria across chow and HFD-fed groups. D: Lipid class abbreviations and color codes. E, F: Distribution of the different lipid classes across chow and HFD conditions. G: Bar graphs depicting the concentration of lipid classes. Each data point in the bar represents ZT0, 4, 8, 12, 16, and 20 for both chow-fed and HFD-fed groups (n = 3 biological replicates generated from 6 mice/ZT point). Data are presented as mean ± SEM. Statistical significance was determined using unpaired Student's *t* test; $*P \leq 0.05$, $***P \leq 0.001$.

cytosolic, nucleus, and endoplasmic reticulum marker protein levels were higher in the lysate of chow- and HFD-fed liver tissue than mitochondrial fraction, ascertaining the purity and enrichment of mitochondria (supplemental Fig. S1A–C).

Next, we employed shotgun lipidomic analyses to profile and quantify membrane lipid species of the mitochondrial fraction. To avoid any artifacts, we generated three biological replicates from six mice/ZT point/diet, sacrificed all mice within 10 min to avoid light-induced changes, and employed a stringent cut-off to select lipid species. Our lipidome identified a total of 405 glycerophospholipid species from mitochondria. Out of these, 127 lipid species with a coefficient of variation ≤0.3 were selected for detailed analyses from all diets and ZT points. Also, we listed all the lipid species that failed to meet our cut-off (Supplemental Excel Sheet 1), and we observed that largely very long chain fatty acids containing phospholipids and ether-linked phospholipid species belonged to this list. We subjected our lipidome data to the principal component analysis, and it showed a distinct pattern between chow- and HFD-fed mitochondria (Fig. 1B). While chow ZT points showed a dispersed pattern across two axes, the HFD ZT points clustered together, suggesting that HFD promoted less variance. Next, we quantified and compared the total mitochondrial lipids synthesized across all ZT points of chow- and HFD-fed liver mitochondria. As anticipated, DIO increased the total polar lipid content significantly (Fig. 1C). While HFD displayed a severe reduction in the fatty acyl chain length of C:30–35 (~25%) and C:55–70 (~45%), HFD increased C:35–55 (~22%) and C:70–80 (~26%) acyl chain length in total phospholipids (supplemental Fig. S1D). Besides, we observed a notable decrease in MUFA and an increase in the PUFA of total phospholipids (supplemental Fig. S1E).

The identified lipid species spanned several phospholipid classes, including LPE, PE, PC, CL, lysocardiolipin (LCL), PA, PS, PI, SM, dihydrosphingomyelin (DSM), ether-linked phosphatidylethanolamine (ePE), and ether-linked phosphatidylcholine (ePC) (Fig. 1D). As reported previously, the mitochondrial lipidome from chow-fed mice constituted predominantly with PC, PE, and PI as a third abundant lipid class (23). The mitochondrial-specific lipid, CL, represented a fourth abundant lipid class in our lipidome analyses. Besides, we also observed significant levels of PS, SM/DSM, ePC, ePE, and PA as a constituent of our mitochondrial lipidome (Fig. 1E, F). Interestingly, PA seemed more susceptible to the HFD challenge, and DIO reduced PA levels drastically by ~45% as compared to chow-fed mice. While LPE, PE, PS, PI, ePE, and SM/DSM phospholipid classes remain unchanged in their total abundance, we observed a significant increase in the total CL and an uptrend of PC and ePC levels upon HFD treatment (Fig. 1G). Together, our data suggested that DIO potentially altered the percentage and the total abundance of individual lipid classes in the liver mitochondria.

### DIO influenced the acyl chain remodeling of mitochondrial membrane lipids in the liver

Glycerophospholipids with varying chain lengths and degrees of saturation/unsaturation generate heterogeneity in the molecular species of phospholipid classes and, thus, can decorate the mitochondrial membrane with an ideal lipid-protein ratio and maintain appropriate fluidity (52). Therefore, we next probed the profile of molecular species of phospholipids to understand the molecular characteristics associated with DIO in the liver. As evident, the heatmap highlighted that DIO drastically altered the abundance of lipid molecular species identified in our study (**Fig. 2**A). Further, our detailed analyses noted that DIO altered chain length distribution and degrees of unsaturation in major phospholipid classes of mitochondria in the liver (Fig. 2B, C). Also, PCA emphasized the distinct differences in mitochondrial lipid classes between chow- and HFD-fed mice liver. Strikingly, the PCA score plot displayed a clear separation for PC and PE, while the 95% confidence ellipses for CL, LCL, and LPE. This result indicated that DIO showed more impact on PC and PE lipid classes than others (supplemental Fig. S2A–E).

Although HFD reduced the overall abundance of LCL (Fig. 2D) and LPE16:1 and 18:2 molecular species (Fig. 2F) by ~40–50%, HFD showed a dichotomy impact on CL, PE, and PC lipid classes. For example, while HFD significantly increased several molecular species of CL (70:5, 72:8, 72:7, 74:8), we detected a striking decline of about ~50% in the abundance of CL species, namely CL 68:6, 70:7, 70:6 (Fig. 2E). However, we discerned a significant change in the composition at the species level and in particular, DIO showed a drastic reduction (~50%) of PE 32:1, 34:3, 34:1, and 36:5 species. Although we noted a significant reduction in PE 36:4, 36:3, 38:5, 38:3, and 40:5 species, DIO exhibited a notable increase in PE 36:2, 38:4, and 40:6 species (Fig. 2G). Similarly, HFD declined the amount of PC species with acyl chain length of C30:0, 32:2, 32:1, 32:0, 34:3, 34:2, 34:1 and significantly increased more than ~40% of the abundant PC species such as 36:1, 38:6, 38:4, 40:8, 40:7, 40:6, 40:4, 42:10, 42:6 (Fig. 2H). These findings underscored the significant remodeling of the mitochondrial lipidome, highlighting specific lipid species and classes that are differentially affected by high-fat diet conditions.

### HFD challenge remodeled mitochondrial phospholipid species

In general, perturbation in the acyl chain remodeling of glycerophospholipids robustly modifies the fluidity of the mitochondrial membrane and affects the efficiency of nutrient oxidation and ATP generation (53–56). As described in the previous section, HFD

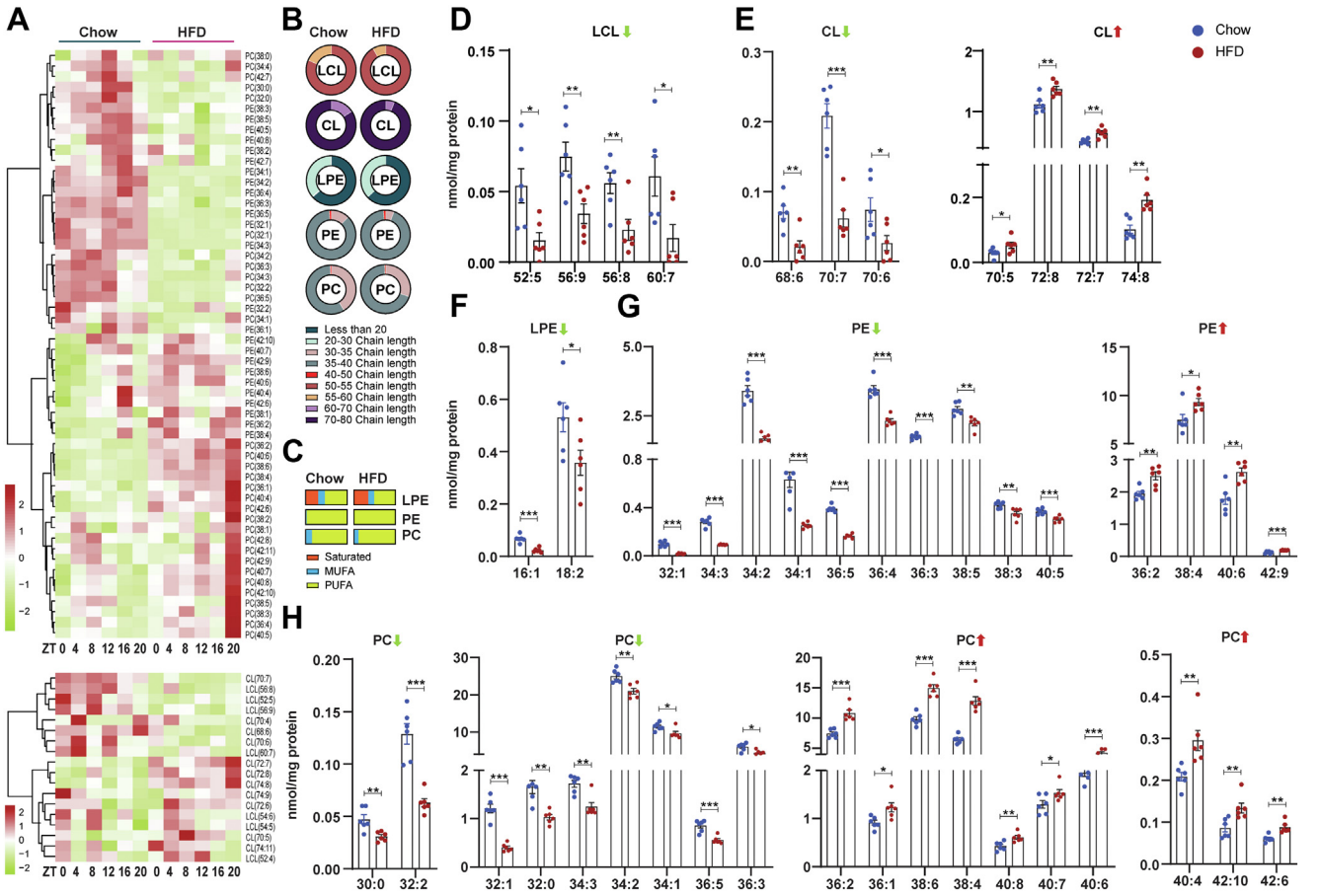


**Fig. 2.** Diet-induced obesity altered phospholipid and cardiolipin profiles. A: Heat map with hierarchical clustering (n = 3 biological replicates generated from 6 mice/ZT point). B: Distribution of acyl chain lengths in LCL, CL, LPE, PE, and PC in the liver mitochondria. C: HFD-induced changes in the degree of fatty acid unsaturation in mitochondrial lipid classes. Relative abundance of different lipid classes (D) LCL, (E) CL, (F) LPE, (G) PE, and (H) PC in the mitochondria of chow and HFD conditions. Each data point on the bars represents a specific ZT point (n = 3 biological replicates/ZT point). Data are presented as mean ± SEM. Statistical significance was determined using two-way ANOVA; $^{*}P \leq 0.05$, $^{**}P \leq 0.01$, $^{***}P \leq 0.001$.

treatment modified the fatty acyl chain length and unsaturation levels in the mitochondrial lipids. Thus, we were intrigued to analyze the impact of HFD on mitochondrial lipidome in greater detail. The heat map showed a distinct pattern of molecular species that are selectively decreased and increased due to DIO across various phospholipid classes (**Fig. 3**A). The PCA analysis revealed partial overlap between chow and HFD groups for PS, PI, and PA, whereas ePC, ePE, and SM exhibited distinct separation (supplemental Fig. S3A–F). While PS showed no significant difference in fatty acyl chain length due to dietary intervention, HFD elevated 35–40 chain length containing PA and ePC species. Also, HFD increased saturated fatty acid-containing SM and PUFA-containing PA and ePE molecules, suggesting acyl chain length and degree of unsaturation were greatly influenced by DIO (Fig. 3B, C). Interestingly, PA molecules seemed to be the most vulnerable phospholipid class to nutrient perturbation, followed by ether-linked phospholipids (Fig. 3D). As evident, HFD diminished PA species of 32:1 and 34:4 by ~75% and on contrary, elevated most ePC species such as ePC34:3, 36:1, 38:6, 38:5, 38:4, 38:2, 40:6, 40:4 (Fig. 3D, H). Besides, we also monitored that HFD significantly reduced various PS species, ePE38:0, ePC32:0, 34:1, and 34:2 species, by ~30% (Fig. 3E, H, I). While HFD decreased minor PI species, we observed heightened levels in major PI38:4 species (Fig. 3F). Additionally, HFD mice displayed higher levels of SM18:0 and SM22:0 species and decreased the levels of SM24:1 and SM24:0 (Fig. 3G). Overall, the HFD challenge accumulated the vast majority of ePC species compared to ePE, PA, PS, PI, and SM (Fig. 3D–I). Together, our data suggested that DIO affected membrane composition by altering the chain length, degree of unsaturation and abundance, and/or the ratio of phospholipid distribution in the mitochondrial membrane.

### HFD modulated the temporal oscillation profile of mitochondrial lipids in the liver

Previous reports suggest that obesity perturbs the internal circadian clock machinery and affects the oscillation pattern of membrane lipid composition in the liver (28–31). Also, an elegant approach using

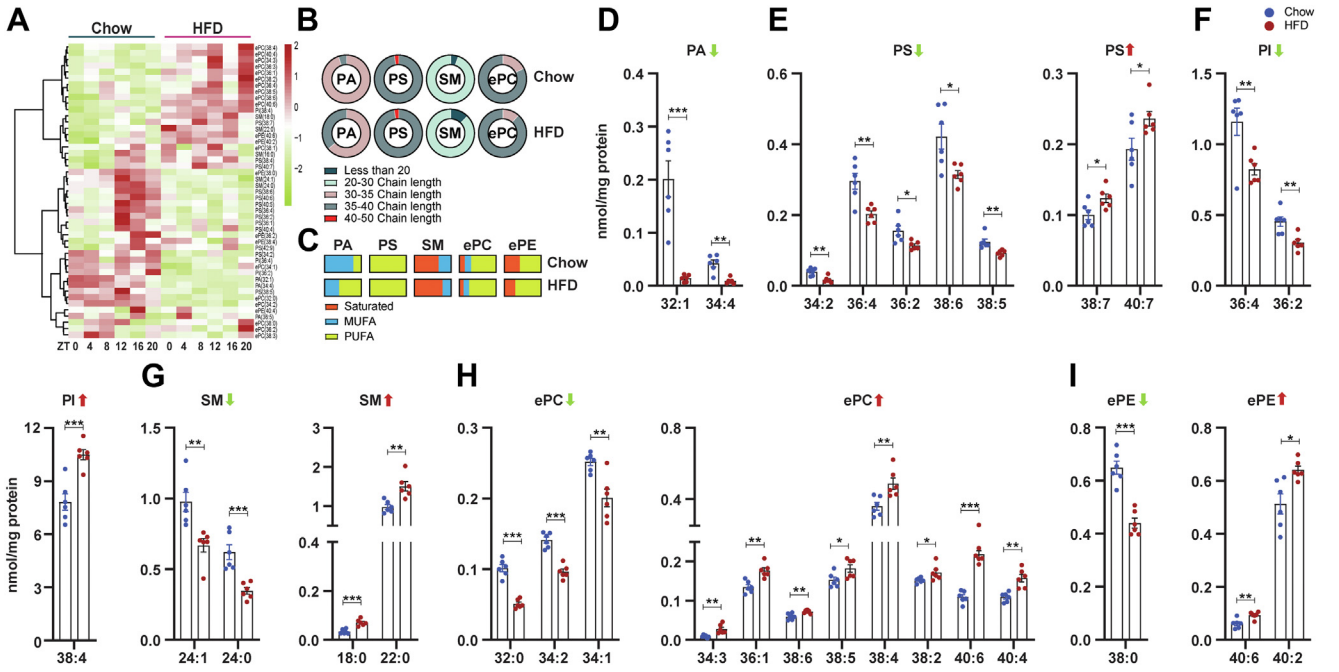


**Fig. 3.** HFD modified phospholipid and ether-linked phospholipid species in the liver mitochondria. A: Heatmap showing changes in lipid species concentrations along with hierarchical clustering. Each column corresponds to specific ZT point (n = 3 biological replicates generated from 6 mice/ZT point). B: Acyl chain length distribution within PA, PS, SM, and ePC species. C: Changes in fatty acid unsaturation levels in PA, PS, SM, ePC, and ePE upon HFD-challenge. D–I: Relative abundance of lipid species (D) PA, (E) PS, (F) PI, (G) SM, (H) ePC, and (I) ePE. Each data point on the bars represents the average lipid concentration of a specific ZT point. Each ZT point contains three independent biological replicates (n = 3 biological replicates generated from 6 mice/ZT point). Data are presented as mean ± SEM. Statistical significance was determined using two-way ANOVA; $^{*}P \leq 0.05$, $^{**}P \leq 0.01$, $^{***}P \leq 0.001$.

quantitative lipidomics unravels the temporal and spatial organization of lipids in the nucleus and mitochondria (23). However, obesity-induced mitochondrial lipid remodeling and whether obesity affects the temporal oscillation pattern of mitochondrial lipidome remains unknown. Therefore, we investigated the impact of DIO on the temporal oscillation of mitochondrial membrane lipid composition using lipidomics analyses. For this approach, we isolated mitochondria from the liver of mice fed with chow and HFD and examined the daily changes of each lipid class and their molecular species at various time points such as ZT0, ZT4, ZT8, ZT12, ZT16, and ZT20. As shown in **Fig. 4**A–J, our data revealed that each lipid class showed a unique pattern of oscillation. Thus, we aimed to analyze and cluster the daily oscillation pattern for each lipid class. We calculated the acrophase for each lipid class using JTK_Cycle analysis. Notably, the abundance of PE, PS, and ePE lipid classes peaks in their abundance during the dark phase at the ZT16 time point in the chow diet. Conversely, HFD hampered the oscillation pattern of these aforementioned lipid classes except PS. For example, the ePE lipid class showed an acrophase at ZT6, and PE peaked at the early light cycle starting from ZT0 in the HFD group. Overall, we profiled mitochondrial lipid species from two different nutritional states and analyzed the temporal organization of various lipid classes. Our data suggested that HFD treatment annulled the oscillation profile of PE, PS, and ePE lipid classes (Fig. 4B, F, J and supplemental Fig. S4A). Besides, DIO significantly decreased the levels of PA across all ZT points and LPE during the late dark phase (supplemental Fig. S4B). Interestingly, PC and ePC species displayed similar temporal profiles in chow-fed mice, peaking at the light phase ZT10 and ZT8, respectively and falling trend during the dark phase, suggesting both lipid classes are coregulated in the biosynthetic process (Fig. 4C, I). Though individual species showed rhythmicity from each lipid class, the total abundance of LPE, PC, PA, PI, CL, SM, and ePC lipid classes showed no circadian rhythmicity as per JTK_Cycle analysis (Fig. 4A, C, D, E, G–I).

Strikingly, the HFD challenge modulated the temporal accumulation profiles of mitochondrial lipid classes. However, molecular species from inter- and intra-lipid classes showed varying patterns in their daily accumulation profile. For instance, several molecular species belonging to the intra-lipid class showed different oscillation profiles, and molecular species belonging to the inter-lipid class displayed a similar pattern of daily oscillation. Hence, we employed unbiased hierarchical clustering and pairwise correlation analyses to group lipid species based on their daily oscillation profile, irrespective of their lipid class. These analyses identified 10 distinct clusters from the mitochondria of chow-fed mice and seven clusters in the

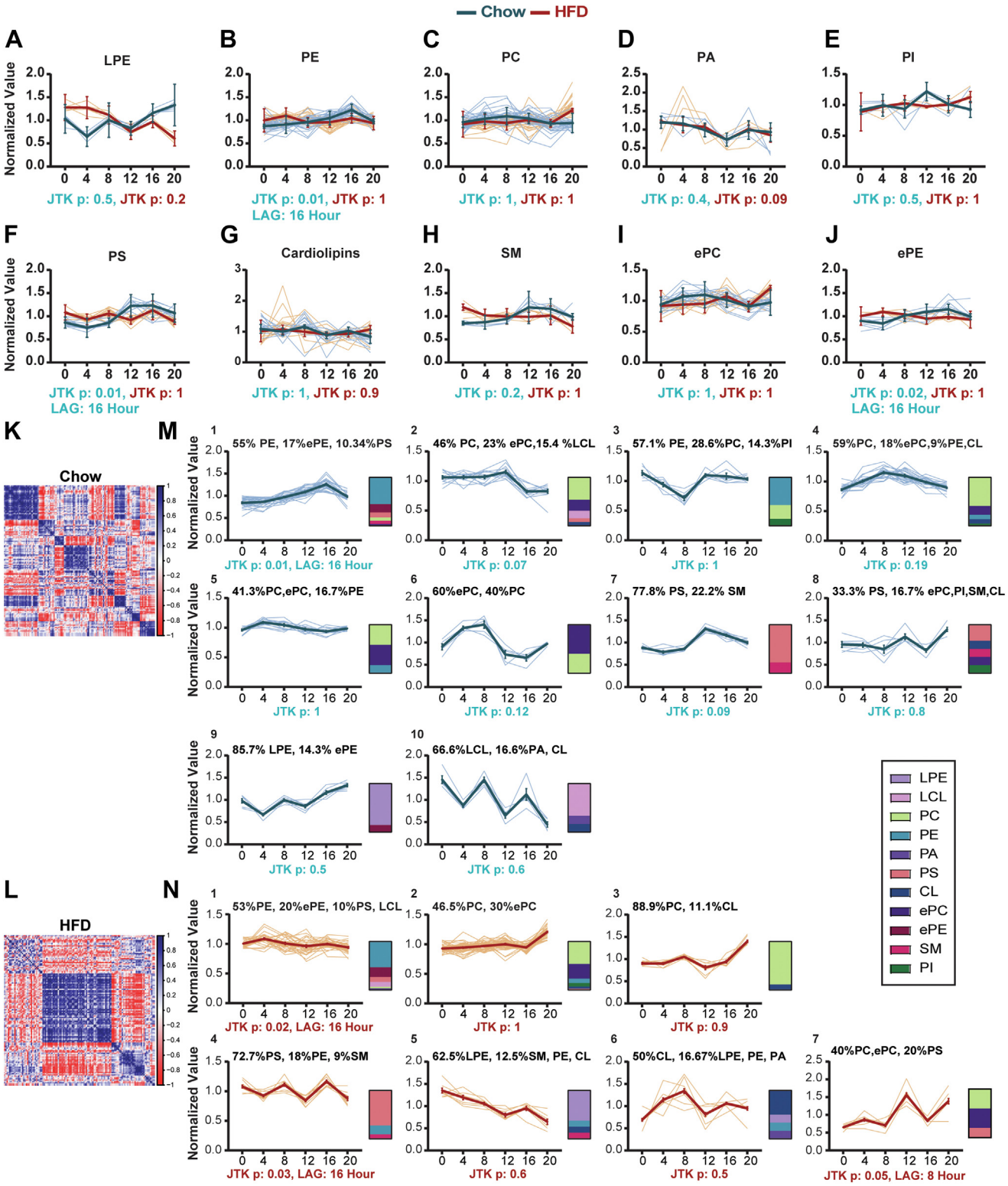


**Fig. 4.** Temporal oscillation and hierarchical clustering of liver mitochondrial lipidome in lean and obese mice. A–J: Temporal profiles of lipid species normalized to their daily means, grouped by lipid classes: (A) LPE, (B) PE, (C) PC, (D) PA, (E) PI, (F) PS, (G) cardiolipins, (H) SM, (I) ePC, and (J) ePE. Thick colored lines indicate the average oscillation profile of each class and thin lines represents the oscillation profile of individual lipid species. Statistical significance of rhythmicity was determined using JTK_CYCLE for the total abundance of each lipid class. K–N: Hierarchical clustering of lipid profiles was performed based on Euclidean distance. Correlation matrix sorted by clusters for (K) chow-fed mitochondria and (L) HFD-fed mitochondria. M, N: Each plot represents daily profile of lipid species based on their hierarchical cluster from (M1-10) chow and (N1-7) HFD-fed mitochondria. Values are normalized to daily mean of each lipid species. Adjacent colored bars indicate the percentage distribution of lipid classes within each cluster. Thick line represents the average oscillation profile of that cluster, and its statistical significance of rhythmicity

HFD-fed mice. Further, it identified that the temporal organization of mitochondrial lipidome appeared more homogeneous in the HFD-fed mice between lipid clusters compared to chow-fed mice (Fig. 4K, L). This data suggested that HFD generated a synchronized lipid oscillation profile, potentially reflecting a uniform adaptation to nutritional stress. Interestingly, we found a single lipid class present in multiple clusters, each exhibiting different oscillation profiles. For instance, PC species appeared in six different clusters in chow-fed mice, with the profiles of these clusters peaking at different ZT points during LD entrainment. On the other hand, PC species from the mitochondria of HFD mice assembled into three different clusters, suggesting that the HFD challenge narrowed the pattern of the temporal accumulation profile of PC species. Conversely, SM species from DIO mice were grouped into three different clusters, while SM species from chow-fed mice were categorized into two different clusters (Fig. 4M, N). Although the chow-fed group showed several distinct clusters, cluster M1 displayed strong circadian rhythmicity with a JTK_Cycle *P*-value of 0.01 and composed of 29 lipid species that majorly fell into PE, ePE, and PS lipid classes. Interestingly, we observed that both class-wise and hierarchical clustering demonstrated that these aforementioned lipid classes showed circadian rhythmicity in chow-fed mice. Conversely, hierarchical clustering showed three clusters with circadian rhythmicity in the HFD-fed group, but cluster N1 composed the vast majority of the lipid species belonging to PE, ePE, PS, and LCL. These findings provided insights into the dynamic organization of the mitochondrial lipidome and highlighted the impact of HFD on selective lipid class rhythmicity. The observed clustering patterns and phase shifts underscored the complexity of lipid metabolism and its differential regulation by the nutritional challenge.

### JTK_Cycle analyses revealed DIO perturbed the diurnal rhythmicity of mitochondrial lipids

To further explore whether HFD influenced the diurnal rhythmicity of mitochondrial lipids, we subjected individual lipid species to the JTK_Cycle algorithm, a nonparametric method designed to identify rhythmic components. Further, we included lipids with coefficients of variation below 0.3 across all diets and time points, serving as our detection limit for our analysis and eliminating potential artifacts. In mitochondria from chow-fed mice, 33 out of 127 lipids exhibited oscillatory behavior, accounting for ~26% of the total lipidome. However, mice fed with HFD decreased this rhythmicity to 9% in mitochondria, with 11 oscillating out of 127 lipids species. We further explored the impact of DIO on individual lipid species and categorized them into four different groups such as (i) oscillating, (ii) nonoscillating, (iii) significant, and (iv) nonsignificant changes in their levels at various ZT points. As shown in the heat map, we noticed that the dietary regimens altered the concentration of both oscillating and nonoscillating species at any one or more ZT points (supplemental Fig. S5A–C). We next probed to evaluate the most entrained lipid class and detected nearly 60% of the rhythmic lipidome of chow-fed mice consisted of PC and PE species, followed by ~18% of PS, ~9% of ePE, ~3% of CL and PI (**Fig. 5**A). Also, we observed a drastic reduction (~65%) in the number of lipid species that displayed rhythmicity upon HFD challenge. However, the distribution of rhythmic lipid classes in the HFD-fed group was distinct as compared to the chow diet, with a predominance of PE and CL species. Also, ePC and LCL lipid classes showed rhythmicity in HFD-fed mice (Fig. 5B). We further investigated whether HFD affected the acrophase of rhythmic lipids in mitochondria. Our analysis revealed that the timing of the peak in lipid abundance differed between chow-fed and HFD-fed mice. In chow-fed mice, most lipids peaked during the dark cycle, whereas in HFD-fed mice, lipid peaks were distributed across the LD cycle, indicating a phase shift (Fig. 5C, E and supplemental Fig. S5A, B). Interestingly, out of the 33 oscillating species in chow-fed mice and 11 in HFD-fed mice, no individual lipid species were found to oscillate in both chow- and HFD-fed groups (Fig. 5E). To our surprise, we observed that most of the PE and PS species showed acrophase between ZT14 to ZT18, while the most abundant membrane lipid PC peaked during the light phase (Fig. 5C, E).

We also analyzed the degree of overlap between oscillating, significant, and nonsignificant lipid species changes in their abundance by diet. As shown in the Ven diagram, 37 lipid species showed both circadian oscillation and significant change in their levels at one or more ZT points, while seven lipid species displayed circadian oscillation without significant change in their levels. Among 37 lipid species, HFD challenge consisted of PE38:1, PE36:3, PE32:2, PC38:2, LCL60:7, ePE38:0, ePC32:0, CL70:6, CL70:5, and CL68:6 and remaining 27 lipid species belonged to chow-fed mitochondria (supplemental Fig. S5D, E). Further, we also probed the distribution of 95 lipid species that are altered significantly in their levels at various ZT points irrespective of their rhythmic profile (supplemental Fig. S5F). However, among 83 nonoscillating lipid species, 58 lipid species differed significantly in their levels at one or more ZT points and the remaining 25 species did not display circadian oscillation or change in the levels by

was determined using JTK_Cycle. LAG corresponds to the acrophase for the 24-h cycle. Thin line depicts the individual lipid species. Statistical significance for JTK_Cycle analysis determined at $P < 0.05$.

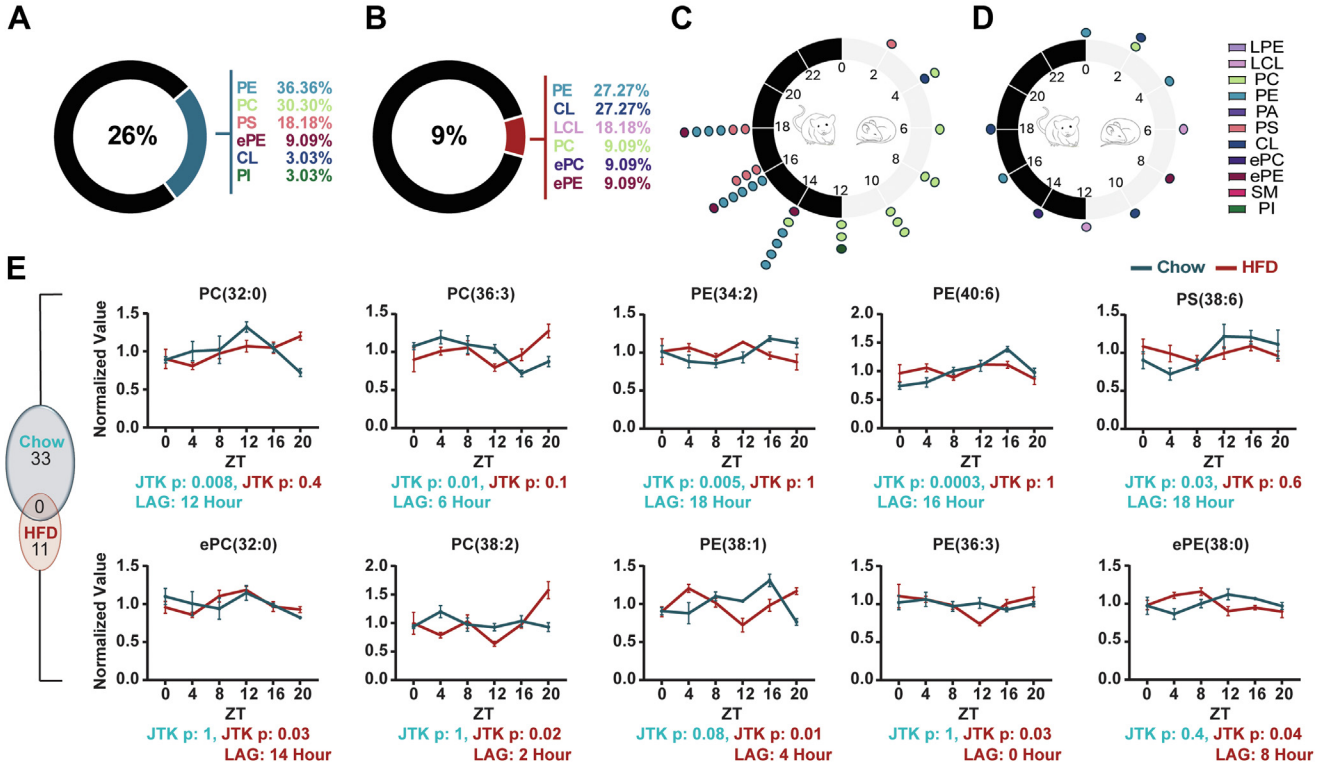


**Fig. 5.** JTK_Cycle analysis displayed distinct temporal lipid profiles in DIO mice. A, B: Proportion of lipids showing circadian oscillations over a 24-h cycle based on JTK_Cycle analysis. The pie charts illustrate the distribution of these entrained lipids by class in (A) chow-fed and (B) HFD-fed mice. C, D: Acrophase distribution of oscillating lipid species in the mitochondria of (C) chow-fed and (D) HFD-challenged mice. Lipids are color-coded by class. E: Venn diagram illustrating lipid species that oscillate exclusively in chow-fed mice, HFD-fed mice, or both, along with normalized daily accumulation profiles of representative lipid species. LAG corresponds to the acrophase for the 24-h cycle. Data are presented as mean ± SEM. Statistical significance of rhythmicity was determined using JTK_Cycle, with statistical significance determined at $P < 0.05$.

dietary intervention. In nonoscillating cum significant lipid species, we noted that the vast majority of PC, ePC, and SM lipid species showed a significant upsurge in their levels by DIO across various ZT points. Interestingly, more PE, PC, PS, LPE, and PA lipids species revealed a significant change in their abundance at one or more ZT points in the chow group (supplemental Fig. S5D, G). Overall, our findings highlighted the profound impact of HFD on the rhythmicity, concentration, and phase of mitochondrial lipids, suggesting potential metabolic reprograming in response to dietary interventions.

### Dietary intervention affected the coregulation of various mitochondrial lipid species

Our analyses revealed the intricate changes in the daily rhythm of mitochondrial lipidome upon high-fat diet feeding. Thus, we arranged lipid species across all lipid classes for pairwise correlation analysis to uncover potential organization patterns that may suggest coregulation of various lipid species. This metric displayed higher correlation values for HFD (median r values of 0.43) as compared to the chow diet (median r values of 0.39). Further, it hinted that positively correlated lipid species were more prevalent in the mitochondria of HFD-fed mice compared to a chow diet (**Fig. 6**A, B). However, these positively correlated lipid species possessed varying acyl-chain lengths and degrees of unsaturation that traverse into inter- and intra-class lipids. As evident, chow mitochondrial lipidome included pairs with higher positive correlations, such as PC(38:6)-PC(38:4), LPE(16:0)-LPE(18:1), and PC(36:4)-ePC(38:5), reflecting similar patterns of daily accumulation. Also, lipid pairs such as PC(34:1)-PC(38:4), PC(34:2)-ePC(40:6), PE(36:4)-PE(38:4), and LPE(16:0)-LPE(18:1) from HFD-fed mice exhibited stronger correlations in their oscillatory profiles, which led us to explore factors that might influence these correlations. Further, our analyses consistently showed that several lipid classes displayed more temporal uniformity despite possessing different fatty acyl-chain lengths and saturations (Fig. 6A–C). Conversely, lipid species within the same class correlated more strongly than inter-class lipid species. Certain lipid classes, like LPE and LCL in the chow diet and PS, SM, and PE in the HFD, showed a greater tendency for within-class correlation, while others, such as PI, were more prone to between-class correlations. Interestingly, both PC and ePC in mitochondria demonstrated a mix of within and between-class correlations (Fig. 6D, E). Overall, we observed that within-class correlations were stronger in the mitochondria of HFD-fed mice (62.12%) than in

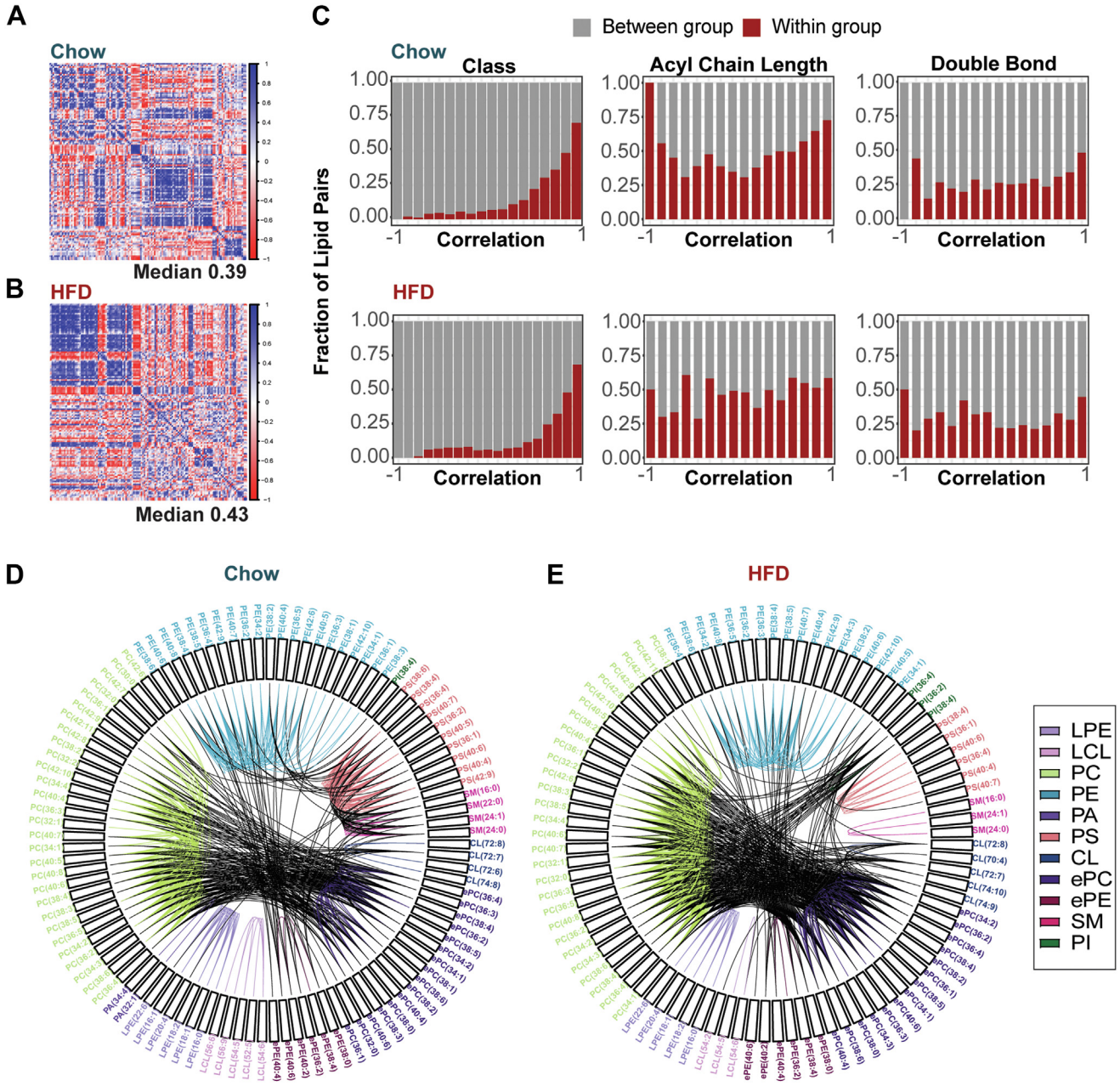


**Fig. 6.** HFD altered lipid correlations and interactions across lipid classes in liver mitochondria. A, B: Correlation matrix sorted by lipid class for (A) chow-fed and (B) HFD-fed mice liver mitochondria. Rows and columns correspond to 127 lipid species identified in the mitochondria with covariance value ≤ 0.3. C: Lipid pairs are grouped based on the strength of their correlations across two diets. These groups are further categorized by lipid class, acyl chain length similarity, and degree of unsaturation. Pairs are distinguished as being within the same lipid class or across different lipid classes. D, E: Network visualization of highly correlated lipid pairs ($r > 0.8$) in (D) chow-fed and (E) HFD-fed liver mitochondria. Each lipid is represented by a node around the circle and color coded according to its class. Within-class correlations are depicted with colored lines according to lipid class, while between-class correlations are shown in *black*. FDR with q value < 0.01.

chow-fed mice (59.57%). These findings suggested how diet impacts the lipid organization profile in mitochondria.

### Circadian oscillation of PE, PC, and PS correlated with mitochondrial function

As reported previously (57–59), the PC/PE ratio and PE deficiency impair oxidative phosphorylation and mitochondrial function. As described earlier in this manuscript, DIO annulled the oscillation of PE, PC, ePE, and PS lipid species, and thus, we analyzed whether DIO dampened the rhythmicity of PE/PC, ePE/PC, and PS/PC ratio to emphasize the interplay between diet-induced temporal re-organization of lipid species and mitochondrial function. Our analysis demonstrated that chow-fed mitochondria displayed rhythmicity and

showed acrophase between ZT14 to ZT18, which is considered to be the most active metabolic phase. Conversely, HFD-induced lipid accumulation in the liver affected the temporal oscillation of these lipid species and their ratio to PC, suggesting mitochondrial lipid oscillation is essential to maintain appropriate membrane composition to execute mitochondrial function (**Fig. 7**A–C). Since the aforementioned lipid classes showed an acrophase between ZT14 to ZT18, we were intrigued to probe whether HFD-induced mitochondrial lipid remodeling correlates to OXPHOS proteins and mitochondrial function. To address this, we examined the levels of OXPHOS complex proteins at ZT4 and ZT16 and noted that chow-fed mice showed elevated levels of OXPHOS proteins, complex II, complex IV, and complex V at ZT16 and correlated with the peak time of PE, PS, and ePE. In contrast, HFD dampened this association and affected the OXPHOS complex protein levels, suggesting that the circadian rhythmicity of these lipids is essential (Fig. 7D, E and supplemental Fig. S7A, B). Further, we evaluated whether the peak time of these lipids was connected with mitochondrial function. For this, we carried out an OCR assay using isolated mitochondria from chow- and HFD-fed mice at ZT4 and ZT16 (Fig. 7I). To corroborate our data with the circadian clock, we next examined the daily rhythmicity of clock genes such as *Bmal1*, *Rev-Erbα*, and *Per2* in the liver of chow- and HFD-treated mice. As reported, DIO significantly changed the daily oscillation of clock genes along with *Srebp1c*, a master regulator of lipid synthesis and other genes involving fatty acid biosynthesis (supplemental Fig. S6A–F). Notably, *Srebp1c* also showed a peak time at ZT14 and reduced during the light cycle, as reported (28, 60). As known, rodents demand high energy during the dark phase (ZT14-18) and our data also aligned well and supported that OCR and rhythmicity of these lipids synchronized in chow-fed mice. Next, we explored how the mitochondrial dynamics and mitophagy processes were entrained in an LD cycle in chow- and HFD-fed mice. We analyzed the protein levels of VDAC, MFN2 (mitochondrial fusion marker), PINK, and Parkin (mitophagy markers) at ZT4 (light phase) and ZT16 (dark phase) (Fig. 7D, F–H and supplemental Fig. S7C). As reported, Parkin-mediated mitophagy is vital to support high energy demand during the dark phase at ZT16. Strikingly, the Parkin level was elevated at ZT16, while PINK1 and VDAC levels were unchanged in chow-fed mice. Conversely, HFD-induced obesity diminished the mitophagy marker, Parkin levels at ZT4 and abolished the increment at ZT16 compared to the chow-fed mice, suggesting the molecular link between the oscillation of mitochondrial lipids and function. Together, our data suggested that dietary intervention perturbed the membrane lipid composition and thus meddled with the correlations between diurnal oscillation patterns of mitochondrial lipids, oxygen consumption rate, and dynamics.

## DISCUSSION

Multiple metabolic processes are tightly coupled with circadian oscillation and the sleep-wake cycle, including food intake, fasting, energy expenditure, and appetite-regulating hormone release. Abdominal obesity with a large neck circumference is not only associated with increased risk for cardiovascular disease and T2DM but is also well connected with circadian misalignment and obstructive sleep apnoea (61). Also, several studies explained that DIO decouples the synchronized function of the central pacemaker and peripheral clocks and accelerates metabolic dysfunction (28, 29, 48–51). Subsequently, obesity induces altered fatty acid flux or metabolites that modulate glucose and lipid homeostasis (30, 46). Besides, high-fat DIO disrupts the circadian clock function by increasing CLOCK and BMAL1 expression (28, 29). BMAL1 deletion is known to cause mitochondrial dysfunction and affects the diurnal oscillation of mitochondrial dynamics (62). PER2 and REV-ERBα are crucial players in regulating circadian rhythm and governing lipid and glucose metabolism. Also, *Per2* or *Rev-erbα* deletion in the liver disrupted the circadian oscillation of lipid metabolism and contributed to metabolic dysfunction, including hepatic lipid accumulation. Also, $Per2^{-/-}$ mice showed disrupted oscillation of lipids during time-restricted feeding in chow-fed mice (23, 24). However, the mechanism at which DIO executes mitochondrial dysfunction and disturbs the daily oscillation of mitochondrial dynamics remains unclear. As reported previously, DIO is known for impeding the transcript levels of clock genes *Per2* and *Rev-erbα* in the liver, followed by impaired lipid oxidation and increased lipid synthesis (28, 29). Our results also demonstrated that DIO decreased the levels of *Per2* and *Rev-erbα*, suggesting their imperative role in mitochondrial lipid composition and function (supplemental Fig. S6B, C).

Although various findings demonstrated the temporal organization of lipids, how DIO influences lipid composition, mitochondrial dynamics, and its oscillation pattern is unknown (23, 63). Therefore, we investigated the effect of DIO on mitochondrial lipid composition and demonstrated that DIO not only changed the lipid profile of mitochondria and dynamics but also affected their oscillation pattern. Among various lipid classes, PA seems more vulnerable to nutritional stress or HFD challenges than other lipid classes. Though HFD did not significantly impact the total levels of individual lipid classes, HFD brought out drastic changes at the individual molecular lipid species level. For example, HFD increased the total abundance of CL, mitochondrial specific lipid class, and PUFA but reduced specific CL species very strikingly (Figs. 1 and 2). Although CL levels are known to determine mitochondrial membrane potential and respiration, elevated levels of CL are likely to correlate with liver mitochondrial dysfunction (33, 37, 48, 53). Aligning with

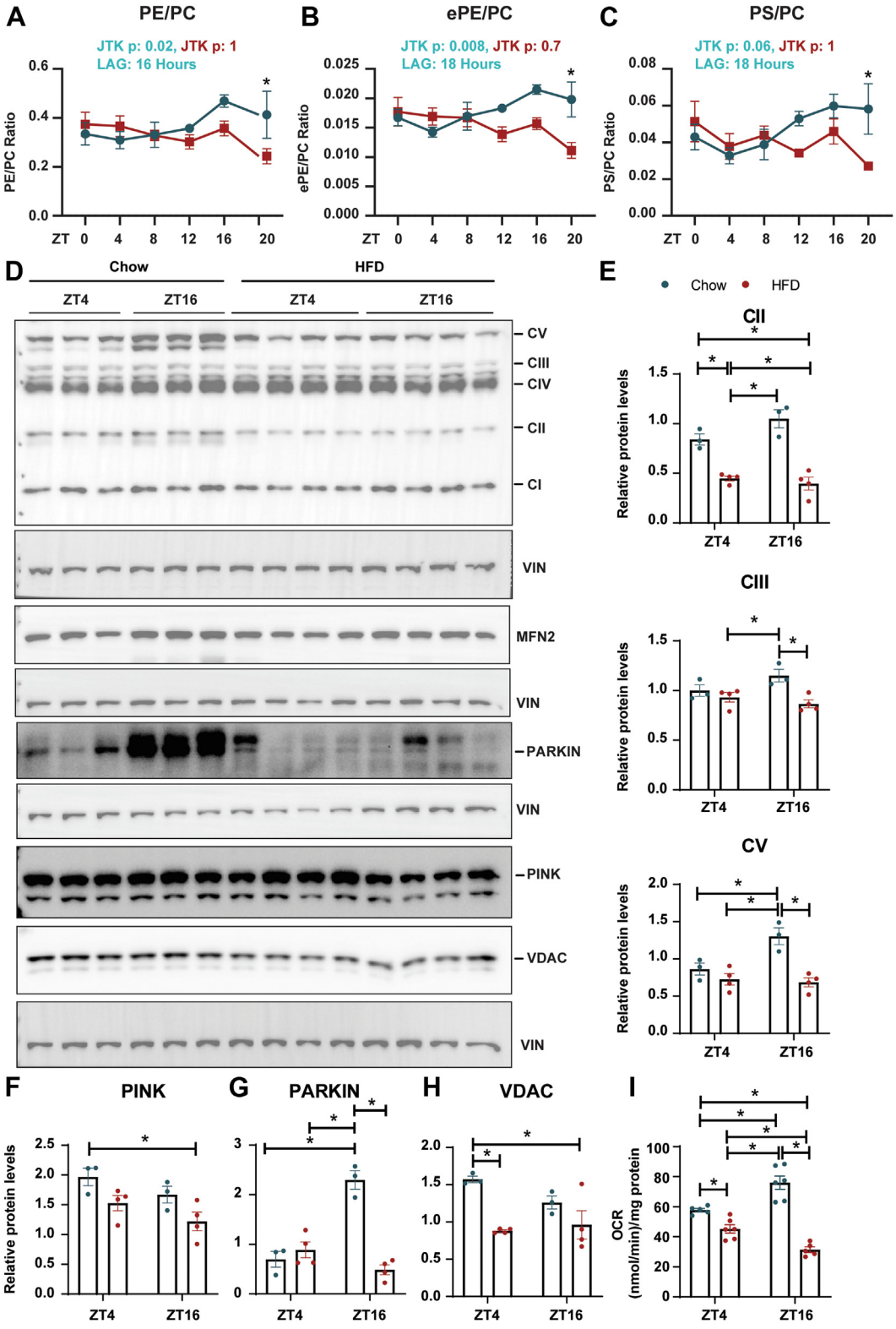


**Fig. 7.** High-fat diet altered the circadian rhythmicity of PE/PC, ePE/PC, and PS/PC. A–C: Oscillation profiles of lipid ratios in liver mitochondria over 24 h in chow and HFD-fed mice: (A) PE/PC ratio, (B) ePE/PC ratio, and (C) PS/PC ratio. D: Immunoblot analysis of OXPHOS complexes, mitochondrial fusion protein MFN2, mitophagy markers PINK1 and Parkin, and VDAC, with vinculin as loading control (n = 3–4 mice/ZT point/group). E–H: Quantification of immunoblot analysis: (E) OXPHOS protein complexes II, III, and V, (F) PINK1, (G) parkin, and (H) VDAC. I: Oxygen consumption rate (OCR) of liver mitochondria isolated from chow and HFD-fed mice at ZT4 and ZT16 (n = 5–6 mice/ZT point/group). Data are presented as mean ± SEM. Statistical significance was determined using two-way ANOVA (*$P \leq 0.05$). LAG corresponds to the acrophase for the 24-h cycle. Statistical significance of rhythmicity was determined using JTK_Cycle, with statistical significance determined at $P < 0.05$.

this, our results support that obesity-induced mitochondrial defect might be due to altered CL composition and distribution of fatty acid symmetry in the membrane. As a known fact, CL with PUFA is prone to oxidation and free radical generation (64). Since CL is part of the electron transport chain (ETC), DIO might have distorted the function by incorporating PUFA in CL and other membrane lipids.

While CL is known to bind tightly onto complex I, PE and PC lightly bind and affect the stability and latter catalytic function, respectively. Besides, PE is part of complex II, III along with CL and complex IV along with PC and CL, suggesting that CL and PE are essential lipids for forming ETC (32–37). Thus, changes in PE and CL could directly contribute to OXPHOS function and control the oxygen consumption rate of liver mitochondria. Our data demonstrated that DIO severely altered the levels of PE and CL molecular species and their acyl chain remodeling during the dark/active phase in the liver. These data suggested that the reduced abundance of several PE species affected the PE/PC ratio and mitochondrial dynamics at ZT16 since more PE species peak between ZT12-16, and they might engaged in forming ETC. Together, our study demonstrated that altered CL and PE levels and their oscillation profile highly corroborated with decreased OXPHOS and OCR levels during DIO. Mitochondrial function and dynamics increase during the dark phase between ZT12-ZT16 or the high energy demand phase, but these processes also generate elevated ROS levels and damaged mitochondria. Thus, PE, PS, CL, and PA are pivotal in activating and regulating the increased mitophagy process to prevent the accumulation of damaged mitochondria (65–67). Our data also correlated with increased mitophagy and PE, PS, CL68:6, CL70:7, LPE16:1, etc. lipids, suggesting that these lipids are engaged with mitophagy during the dark to accompany high energy demand.

Also, DIO selectively increased or decreased the abundance of specific PE, PC, and SM species (Figs. 2 and 3). In particular, HFD decreased the abundance of long-chain fatty acids (<C:36) and increased very long-chain fatty acids (>C:38) containing phospholipids, including PC, PE, PI, ePC, and PS. Our data suggests HFD could diminish the efficiency of very long chain fatty acid (VLCFA) oxidation and, thus, accumulate in different lipid classes, leading to defective mitochondrial membrane formation (Figs. 2 and 3) (68). Additionally, a reduction in PE and PC species could have led to a concomitant decrease in OXPHOS complex IV activity (69). Though several studies dealt with the lipidome of whole cell lysate, our study specifically cataloged the lipid species of mitochondria and demonstrated that DIO accumulated VLCFA-containing phospholipids and ether lipid species in the hepatic mitochondria (30, 31).

As acquainted, mitochondria are an indispensable organelle in maintaining cellular energy homeostasis and thus, mitochondrial composition, dynamics, and quality control are under strict regulation. However, several metabolic and/or environmental cues strongly impact membrane lipid composition. Mitochondrial lipids contribute a major share in determining the physicochemical properties of mitochondrial membrane fluidity, curvature, lipid-protein ratio, assembly of supramolecular protein complexes, etc (23, 38, 48, 50, 51, 53, 54). In line with this phenomenon, our study also revealed that a reduction in the number of diurnally oscillating lipid species, in specific PE and PS phospholipids strongly associated with mitochondrial morphology and membrane fusion, as one of the striking impacts of HFD treatment (Figs. 4 and 5). The oscillating PE species under both diet conditions had similar acyl chain lengths (C32–C41), suggesting the DIO-generated modulation in the proportion of PUFA and VLCFA affected the temporal rhythm of mitochondrial lipid remodeling in the liver. Also, the reduction in PS oscillation likely contributed to the observed decrease in PE oscillatory behavior since PE synthesis depends on an enzymatic decarboxylation of PS (70). Besides, our hierarchical clustering analysis further endorsed that HFD reduced the diversity of lipid molecular species overall and, thus, led to the reduced number of oscillating molecules and generated a phase shift in the diurnal rhythm of PE species, a definite phase shift. For example, HFD treatment increased interclass correlations, indicating a shift toward greater lipid homogeneity in certain lipid classes, such as PS, oscillations reverted to intraclass correlation under HFD, a sign of disrupted lipid interactions and functions (Fig. 6). Although PE is a major nonbilayer-forming phospholipid in mitochondrial membranes, the temporal oscillation of PE, ePE, and PS species might play a key role in mitochondrial morphology, biogenesis, dynamics, and maintenance (32).

Further, to address the distinct mitochondrial lipid signature during circadian rhythmicity, we integrated the data set available (already published) from whole tissue lysate lipidome with our mitochondrial lipidome (71–74). This analysis led us to identify 62 common lipid species between both data sets and 65 lipid species unique to our mitochondrial data set (data not shown). Also, we detangled the oscillation pattern of these common species and found that the majority of PE species showed rhythmicity only in mitochondria, while more PC species showed rhythmic oscillation in tissue lysate. Further, our analysis revealed that 65 lipid species specific to mitochondria majorly belonged to ePC, CL, PE, PC, LPE, and ePE. Notably, ePC and ePE species were also enriched despite their being minor constituents of mitochondria since other data sets did not explore or even identify these lipid classes in lipidomics. Together, the integrated analyses of common

as well as unique lipid species identified from previously published tissue lysate and our mitochondrial lipidomics data set revealed a greater number of lipid species from PE displayed circadian rhythmicity in mitochondria. However, DIO perturbed this mitochondrial-specific lipid oscillation and their levels across various ZT points, suggesting mitochondrial-specific lipid signature is indispensable to maintain mitochondrial function and dynamics.

It is important to note that the mitochondrial lipidome analyzed in our study reflects mitochondria derived from a heterogeneous population of liver cells. While changes in hepatocyte mitochondria are central to metabolic adaptations in the context of DIO, mitochondria from other liver cell types—such as Kupffer cells, endothelial cells, and hepatic stellate cells—also play critical roles in metabolic stress. During the progression of fatty liver disease, activated Kupffer cells and Stellate cells accumulate triacylglycerol and sphingolipids to promote an inflammatory environment (75). While activated stellate cells showed a decrease in saturated PC, SM, and PA lipid species, they also showed an increase in PS and ePC species (76). Our lipidome data also displayed a certain degree of similarity in decreasing saturated PC and PA species. Also, we noted an increase in several ePCs, PS38:7, and PS40:7 species during DIO, suggesting an overlap between hepatocytes, stellate, and Kupffer cells in the liver. Although our data overlaps with other cell types residing in the liver, further studies comparing mitochondrial lipidomes from specific cell types may contribute valuable insights into the cell type–specific lipid composition and their role in mitochondrial dysfunction in DIO. Altogether, our data suggested that the HFD challenge drastically altered the mitochondrial lipid remodeling and temporal oscillation of lipid species, highlighting the critical role of mitochondrial lipid oscillation in maintaining mitochondrial integrity and function.

## Data availability

Data will be made available on request.

*Supplemental data*

This article contains supplemental data.

*Acknowledgments*

We also thank the CSIR Fellowship (Rashi Jain). We thank Mr. Vishal for all his technical help with the western blots. Also, we thank all members of the lab for assisting in mice dissection at various ZT points.

*Author contributions*

R. J. and R. R. methodology; R. J. and S. R. formal analysis; R. J. and S. R. data curation; R. R. and S. R. validation; S. R. writing–review and editing; S. R. writing–original draft; S. R. supervision; S. R. resources; S. R. project administration; S. R. funding acquisition; S. R. conceptualization.

*Funding and additional information*

This study was supported by Wellcome Trust/DBT India Alliance Fellowship/Grant [IA/I/16/2/502735] and financial support from IISc (S. Rajakumari).

*Conflicts of interests*

The authors declare that they have no conflicts of interests with the contents of this article.

*Abbreviations*

CL, cardiolipin; DIO, diet-induced obesity; DSM, dihydrosphingomyelin; ePC, ether-linked phosphatidylcholine; ePE, ether-linked phosphatidylethanolamine; HFD, high fat diet; LCL, lysocardiolipin; LD, light-dark; LPE, lysophosphatidylethanolamine; MFN2, mitofusin 2; OCR, oxygen consumption rate; OXPHOS, oxidative phosphorylation; PA, phosphatidic acid; PC, phosphatidylcholine; PCA, principal component analysis; PE, phosphatidylethanolamine; PI, phosphatidylinositol; PINK1, PTEN-induced kinase 1; PS, phosphatidylserine; SCN, suprachiasmatic nucleus; SM, sphingomyelin; VDAC, voltage-dependent anion-selective channel; VLCFA, very long chain fatty acid; ZT, Zeitgeber time.

Manuscript received December 13, 2024, and in revised form February 25, 2025. Published, JLR Papers in Press, April 1, 2025, https://doi.org/10.1016/j.jlr.2025.100790

## REFERENCES

1. Hastings, M. H., Field, M. D., Maywood, E. S., Weaver, D. R., and Reppert, S. M. (1999) Differential regulation of mPER1 and mTIM proteins in the mouse suprachiasmatic nuclei: new insights into a core clock mechanism. *J. Neurosci.* **19**, RC11
2. Patton, A. P., and Hastings, M. H. (2023) The mammalian circadian time-keeping system. *J. Huntingtons Dis.* **12**, 91–104
3. Moore, R. Y., Speh, J. C., and Card, J. P. (1995) The retinohypothalamic tract originates from a distinct subset of retinal ganglion cells. *J. Comp. Neurol.* **352**, 351–366
4. Johnson, R. F., Moore, R. Y., and Morin, L. P. (1988) Loss of entrainment and anatomical plasticity after lesions of the hamster retinohypothalamic tract. *Brain Res.* **460**, 297–313
5. Kohsaka, A., and Bass, J. (2007) A sense of time: how molecular clocks organize metabolism. *Trends Endocrinol. Metab.* **18**, 4–11
6. Marcheva, B., Ramsey, K. M., Buhr, E. D., Kobayashi, Y., Su, H., Ko, C. H., *et al.* (2010) Disruption of the clock components CLOCK and BMAL1 leads to hypoinsulinaemia and diabetes. *Nature.* **466**, 627–631
7. Paschos, G. K., Ibrahim, S., Song, W. L., Kunieda, T., Grant, G., Reyes, T. M., *et al.* (2012) Obesity in mice with adipocyte-specific deletion of clock component Arntl. *Nat. Med.* **18**, 1768–1777
8. Rudic, R. D., McNamara, P., Curtis, A. M., Boston, R. C., Panda, S., Hogenesch, J. B., *et al.* (2004) BMAL1 and CLOCK, two essential components of the circadian clock, are involved in glucose homeostasis. *PLoS Biol.* **2**, e377
9. Gekakis, N., Staknis, D., Nguyen, H. B., Davis, F. C., Wilsbacher, L. D., King, D. P., *et al.* (1998) Role of the CLOCK protein in the mammalian circadian mechanism. *Science.* **280**, 1564–1569
10. Hogenesch, J. B., Gu, Y. Z., Jain, S., and Bradfield, C. A. (1998) The basic-helix-loop-helix-PAS orphan MOP3 forms transcriptionally active complexes with circadian and hypoxia factors. *Proc. Natl. Acad. Sci. U. S. A.* **95**, 5474–5479
11. Reick, M., Garcia, J. A., Dudley, C., and McKnight, S. L. (2001) NPAS2: an analog of clock operative in the mammalian forebrain. *Science.* **293**, 506–509
12. Shi, S., Hida, A., McGuinness, O. P., Wasserman, D. H., Yamazaki, S., and Johnson, C. H. (2010) Circadian clock gene Bmal1 is not essential; functional replacement with its paralog, Bmal2. *Curr. Biol.* **20**, 316–321

13. van der Horst, G. T., Muijtjens, M., Kobayashi, K., Takano, R., Kanno, S., Takao, M., *et al.* (1999) Mammalian Cry1 and Cry2 are essential for maintenance of circadian rhythms. *Nature.* **398**, 627–630
14. Zheng, B., Albrecht, U., Kaasik, K., Sage, M., Lu, W., Vaishnav, S., *et al.* (2001) Nonredundant roles of the mPer1 and mPer2 genes in the mammalian circadian clock. *Cell.* **105**, 683–694
15. Duong, H. A., Robles, M. S., Knutti, D., and Weitz, C. J. (2011) A molecular mechanism for circadian clock negative feedback. *Science.* **332**, 1436–1439
16. Kume, K., Zylka, M. J., Sriram, S., Shearman, L. P., Weaver, D. R., Jin, X., *et al.* (1999) mCRY1 and mCRY2 are essential components of the negative limb of the circadian clock feedback loop. *Cell.* **98**, 193–205
17. Akashi, M., and Takumi, T. (2005) The orphan nuclear receptor RORalpha regulates circadian transcription of the mammalian core-clock Bmall. *Nat. Struct. Mol. Biol.* **12**, 441–448
18. Guillaumond, F., Dardente, H., Giguere, V., and Cermakian, N. (2005) Differential control of Bmall circadian transcription by REV-ERB and ROR nuclear receptors. *J. Biol. Rhythms.* **20**, 391–403
19. Preitner, N., Damiola, F., Lopez-Molina, L., Zakany, J., Duboule, D., Albrecht, U., *et al.* (2002) The orphan nuclear receptor REV-ERBalpha controls circadian transcription within the positive limb of the mammalian circadian oscillator. *Cell.* **110**, 251–260
20. Sato, T. K., Panda, S., Miraglia, L. J., Reyes, T. M., Rudic, R. D., McNamara, P., *et al.* (2004) A functional genomics strategy reveals Rora as a component of the mammalian circadian clock. *Neuron.* **43**, 527–537
21. Liu, C., Li, S., Liu, T., Borjigin, J., and Lin, J. D. (2007) Transcriptional coactivator PGC-1alpha integrates the mammalian clock and energy metabolism. *Nature.* **447**, 477–481
22. Raghuram, S., Stayrook, K. R., Huang, P., Rogers, P. M., Nosie, A. K., McClure, D. B., *et al.* (2007) Identification of heme as the ligand for the orphan nuclear receptors REV-ERBalpha and REV-ERBbeta. *Nat. Struct. Mol. Biol.* **14**, 1207–1213
23. Aviram, R., Manella, G., Kopelman, N., Neufeld-Cohen, A., Zwighaft, Z., Elimelech, M., *et al.* (2016) Lipidomics analyses reveal temporal and spatial lipid organization and uncover daily oscillations in intracellular organelles. *Mol. Cell.* **62**, 636–648
24. Gooley, J. J. (2016) Circadian regulation of lipid metabolism. *Proc. Nutr. Soc.* **75**, 440–450
25. Li, M. D., Li, C. M., and Wang, Z. (2012) The role of circadian clocks in metabolic disease. *Yale J. Biol. Med.* **85**, 387–401
26. Yang, X., Downes, M., Yu, R. T., Bookout, A. L., He, W., Straume, M., *et al.* (2006) Nuclear receptor expression links the circadian clock to metabolism. *Cell.* **126**, 801–810
27. Zhong, X., Yu, J., Frazier, K., Weng, X., Li, Y., Cham, C. M., *et al.* (2018) Circadian clock regulation of hepatic lipid metabolism by modulation of m(6)A mRNA methylation. *Cell Rep.* **25**, 1816–18128.e4
28. Eckel-Mahan, K. L., Patel, V. R., de Mateo, S., Orozco-Solis, R., Ceglia, N. J., Sahar, S., *et al.* (2013) Reprogramming of the circadian clock by nutritional challenge. *Cell.* **155**, 1464–1478
29. Kohsaka, A., Laposky, A. D., Ramsey, K. M., Estrada, C., Joshu, C., Kobayashi, Y., *et al.* (2007) High-fat diet disrupts behavioral and molecular circadian rhythms in mice. *Cell Metab.* **6**, 414–421
30. Nam, M., Choi, M. S., Jung, S., Jung, Y., Choi, J. Y., Ryu, D. H., *et al.* (2015) Lipidomic profiling of liver tissue from obesity-prone and obesity-resistant mice fed a high fat diet. *Sci. Rep.* **5**, 16984
31. Mouskeftara, T., Deda, O., Papadopoulos, G., Chatzigeorgiou, A., and Gika, H. (2024) Lipidomic analysis of liver and adipose tissue in a high-fat diet-induced non-alcoholic fatty liver disease mice model reveals alterations in lipid metabolism by weight loss and aerobic exercise. *Molecules.* **29**, 1494
32. Martensson, C. U., Doan, K. N., and Becker, T. (2017) Effects of lipids on mitochondrial functions. *Biochim. Biophys. Acta Mol. Cell Biol. Lipids.* **1862**, 102–113
33. Jiang, F., Ryan, M. T., Schlame, M., Zhao, M., Gu, Z., Klingenberg, M., *et al.* (2000) Absence of cardiolipin in the crd1 null mutant results in decreased mitochondrial membrane potential and reduced mitochondrial function. *J. Biol. Chem.* **275**, 22387–22394
34. Wenz, T., Hielscher, R., Hellwig, P., Schagger, H., Richers, S., and Hunte, C. (2009) Role of phospholipids in respiratory cytochrome bc(1) complex catalysis and supercomplex formation. *Biochim. Biophys. Acta.* **1787**, 609–616
35. Daum, G. (1985) Lipids of mitochondria. *Biochim. Biophys. Acta.* **822**, 1–42
36. Brandner, K., Mick, D. U., Frazier, A. E., Taylor, R. D., Meisinger, C., and Rehling, P. (2005) Taz1, an outer mitochondrial membrane protein, affects stability and assembly of inner membrane protein complexes: implications for Barth Syndrome. *Mol. Biol. Cell.* **16**, 5202–5214
37. Dudek, J., Cheng, I. F., Balleininger, M., Vaz, F. M., Streckfuss-Bomeke, K., Hubscher, D., *et al.* (2013) Cardiolipin deficiency affects respiratory chain function and organization in an induced pluripotent stem cell model of Barth syndrome. *Stem Cell Res.* **11**, 806–819
38. Rajakumari, S., and Srivastava, S. (2021) Aging and beta3-adrenergic stimulation alter mitochondrial lipidome of adipose tissue. *Biochim. Biophys. Acta Mol. Cell Biol. Lipids.* **1866**, 158922
39. Bligh, E. G., and Dyer, W. J. (1959) A rapid method of total lipid extraction and purification. *Can. J. Biochem. Physiol.* **37**, 911–917
40. Zhou, X., Mao, J., Ai, J., Deng, Y., Roth, M. R., Pound, C., *et al.* (2012) Identification of plasma lipid biomarkers for prostate cancer by lipidomics and bioinformatics. *PLoS One.* **7**, e48889
41. Fruehan, C., Johnson, D., and Welti, R. (2018) LipidomeDB data calculation environment has been updated to process direct-infusion multiple reaction monitoring data. *Lipids.* **53**, 1019–1020
42. Zhou, Z., Marepally, S. R., Nune, D. S., Pallakollu, P., Ragan, G., Roth, M. R., *et al.* (2011) LipidomeDB data calculation environment: online processing of direct-infusion mass spectral data for lipid profiles. *Lipids.* **46**, 879–884
43. Brugger, B., Erben, G., Sandhoff, R., Wieland, F. T., and Lehmann, W. D. (1997) Quantitative analysis of biological membrane lipids at the low picomole level by nano-electrospray ionization tandem mass spectrometry. *Proc. Natl. Acad. Sci. U. S. A.* **94**, 2339–2344
44. Welti, R., Li, W., Li, M., Sang, Y., Biesiada, H., Zhou, H. E., *et al.* (2002) Profiling membrane lipids in plant stress responses. Role of phospholipase D alpha in freezing-induced lipid changes in Arabidopsis. *J. Biol. Chem.* **277**, 31994–32002
45. Xiao, S., Gao, W., Chen, Q. F., Chan, S. W., Zheng, S. X., Ma, J., *et al.* (2010) Overexpression of Arabidopsis acyl-CoA binding protein ACBP3 promotes starvation-induced and age-dependent leaf senescence. *Plant Cell.* **22**, 1463–1482
46. Rajendran, R., Suman, S., Divakaran, S. J., Swatikrishna, S., Tripathi, P., Jain, R., *et al.* (2024) Sesaminol alters phospholipid metabolism and alleviates obesity-induced NAFLD. *FASEB J.* **38**, e23835
47. Hughes, M. E., Hogenesch, J. B., and Kornacker, K. (2010) JTK_CYCLE: an efficient nonparametric algorithm for detecting rhythmic components in genome-scale data sets. *J. Biol. Rhythms.* **25**, 372–380
48. Li, J., Romestaing, C., Han, X., Li, Y., Hao, X., Wu, Y., *et al.* (2010) Cardiolipin remodeling by ALCAT1 links oxidative stress and mitochondrial dysfunction to obesity. *Cell Metab.* **12**, 154–165
49. Zheng, P., Ma, W., Gu, Y., Wu, H., Bian, Z., Liu, N., *et al.* (2023) High-fat diet causes mitochondrial damage and downregulation of mitofusin-2 and optic atrophy-1 in multiple organs. *J. Clin. Biochem. Nutr.* **73**, 61–76
50. Togo, M., Konari, N., Tsukamoto, M., Kimoto, R., Yamaguchi, T., Takeda, H., *et al.* (2018) Effects of a high-fat diet on superoxide anion generation and membrane fluidity in liver mitochondria in rats. *J. Int. Soc. Sports Nutr.* **15**, 13
51. Xia, W., Veeragandham, P., Cao, Y., Xu, Y., Rhyne, T. E., Qian, J., *et al.* (2024) Obesity causes mitochondrial fragmentation and dysfunction in white adipocytes due to RalA activation. *Nat. Metab.* **6**, 273–289
52. Hishikawa, D., Hashidate, T., Shimizu, T., and Shindou, H. (2014) Diversity and function of membrane glycerophospholipids generated by the remodeling pathway in mammalian cells. *J. Lipid Res.* **55**, 799–807
53. Pennington, E. R., Funai, K., Brown, D. A., and Shaikh, S. R. (2019) The role of cardiolipin concentration and acyl chain composition on mitochondrial inner membrane molecular organization and function. *Biochim. Biophys. Acta Mol. Cell Biol. Lipids.* **1864**, 1039–1052
54. Monteiro, J. P., Pereira, C. V., Silva, A. M., Maciel, E., Baldeiras, I., Peixoto, F., *et al.* (2013) Rapeseed oil-rich diet alters hepatic mitochondrial membrane lipid composition and disrupts bioenergetics. *Arch. Toxicol.* **87**, 2151–2163
55. Schenkel, L. C., and Bakovic, M. (2014) Formation and regulation of mitochondrial membranes. *Int. J. Cell Biol.* **2014**, 709828

56. Schumacher, M. M., Choi, J. Y., and Voelker, D. R. (2002) Phosphatidylserine transport to the mitochondria is regulated by ubiquitination. *J. Biol. Chem.* **277**, 51033–51042
57. Tasseva, G., Bai, H. D., Davidescu, M., Haromy, A., Michelakis, E., and Vance, J. E. (2013) Phosphatidylethanolamine deficiency in Mammalian mitochondria impairs oxidative phosphorylation and alters mitochondrial morphology. *J. Biol. Chem.* **288**, 4158–4173
58. Birner, R., Burgermeister, M., Schneiter, R., and Daum, G. (2001) Roles of phosphatidylethanolamine and of its several biosynthetic pathways in Saccharomyces cerevisiae. *Mol. Biol. Cell.* **12**, 997–1007
59. Becker, T., Horvath, S. E., Bottinger, L., Gebert, N., Daum, G., and Pfanner, N. (2013) Role of phosphatidylethanolamine in the biogenesis of mitochondrial outer membrane proteins. *J. Biol. Chem.* **288**, 16451–16459
60. Guan, D., Xiong, Y., Borck, P. C., Jang, C., Doulias, P. T., Papazyan, R., *et al.* (2018) Diet-induced circadian enhancer remodeling synchronizes opposing hepatic lipid metabolic processes. *Cell.* **174**, 831–842.e12
61. Chaput, J. P., McHill, A. W., Cox, R. C., Broussard, J. L., Dutil, C., da Costa, B. G. G., *et al.* (2023) The role of insufficient sleep and circadian misalignment in obesity. *Nat. Rev. Endocrinol.* **19**, 82–97
62. Jacobi, D., Liu, S., Burkewitz, K., Kory, N., Knudsen, N. H., Alexander, R. K., *et al.* (2015) Hepatic Bmal1 regulates rhythmic mitochondrial dynamics and promotes metabolic fitness. *Cell Metab.* **22**, 709–720
63. Held, N. M., Buijink, M. R., Elfrink, H. L., Kooijman, S., Janssens, G. E., Luyf, A. C. M., *et al.* (2021) Aging selectively dampens oscillation of lipid abundance in white and brown adipose tissue. *Sci. Rep.* **11**, 5932
64. Paradies, G., Petrosillo, G., Paradies, V., and Ruggiero, F. M. (2009) Role of cardiolipin peroxidation and Ca2+ in mitochondrial dysfunction and disease. *Cell Calcium.* **45**, 643–650
65. Chu, C. T., Ji, J., Dagda, R. K., Jiang, J. F., Tyurina, Y. Y., Kapralov, A. A., *et al.* (2013) Cardiolipin externalization to the outer mitochondrial membrane acts as an elimination signal for mitophagy in neuronal cells. *Nat. Cell Biol.* **15**, 1197–1205
66. Lin, C. C., Yan, J., Kapur, M. D., Norris, K. L., Hsieh, C. W., Huang, D., *et al.* (2022) Parkin coordinates mitochondrial lipid remodeling to execute mitophagy. *EMBO Rep.* **23**, e55191
67. Rockenfeller, P., Koska, M., Pietrocola, F., Minois, N., Knittelfelder, O., Sica, V., *et al.* (2015) Phosphatidylethanolamine positively regulates autophagy and longevity. *Cell Death Differ.* **22**, 499–508
68. Ruiz, M., Cuillerier, A., Daneault, C., Deschenes, S., Frayne, I. R., Bouchard, B., *et al.* (2019) Lipidomics unveils lipid dyshomeostasis and low circulating plasmalogens as biomarkers in a monogenic mitochondrial disorder. *JCI Insight.* **4**, e123231
69. Shinzawa-Itoh, K., Aoyama, H., Muramoto, K., Terada, H., Kurauchi, T., Tadehara, Y., *et al.* (2007) Structures and physiological roles of 13 integral lipids of bovine heart cytochrome c oxidase. *EMBO J.* **26**, 1713–1725
70. Vance, J. E. (2015) Phospholipid synthesis and transport in mammalian cells. *Traffic.* **16**, 1–18
71. Adamovich, Y., Rousso-Noori, L., Zwighaft, Z., Neufeld-Cohen, A., Golik, M., Kraut-Cohen, J., *et al.* (2014) Circadian clocks and feeding time regulate the oscillations and levels of hepatic triglycerides. *Cell Metab.* **19**, 319–330
72. Dyar, K. A., Lutter, D., Artati, A., Ceglia, N. J., Liu, Y., Armenta, D., *et al.* (2018) Atlas of circadian metabolism reveals system-wide coordination and communication between clocks. *Cell.* **174**, 1571–1585.e11
73. Kent, B. A., Rahman, S. A., St Hilaire, M. A., Grant, L. K., Ruger, M., Czeisler, C. A., *et al.* (2022) Circadian lipid and hepatic protein rhythms shift with a phase response curve different than melatonin. *Nat. Commun.* **13**, 681
74. Sprenger, R. R., Hermansson, M., Neess, D., Becciolini, L. S., Sorensen, S. B., Fagerberg, R., *et al.* (2021) Lipid molecular timeline profiling reveals diurnal crosstalk between the liver and circulation. *Cell Rep.* **34**, 108710
75. Neyrinck, A. M., Taper, H. S., Gevers, V., Declerck, B., and Delzenne, N. M. (2002) Inhibition of Kupffer cell activity induces hepatic triglyceride synthesis in fasted rats, independent of lipopolysaccharide challenge. *J. Hepatol.* **36**, 466–473
76. Molenaar, M. R., Haaker, M. W., Vaandrager, A. B., Houweling, M., and Helms, J. B. (2023) Lipidomic profiling of rat hepatic stellate cells during activation reveals a two-stage process accompanied by increased levels of lysosomal lipids. *J Biol Chem.* **299**, 103042